Lewis, M.J., Ryan-Davis, J.R., and Bucholz, C.E., 2023, Mafic Intrusions Record Mantle Inputs and Crustal Thickness in the Eastern Sierra Nevada Batholith: GSA Bulletin, https://doi.org/10.1130/B36646.1.

Supplemental Material

Table S1. Summary of new geochronology in the Eastern SNB.

Table S2. All LA-ICPMS analyses of zircon.

Table S3. XRF data.

Table S4. Averages of the most primitive population of analyses from each mafic body and calculated parental melt compositions.

Table S5. All olivine, clinopyroxene, and orthopyroxene analyses (collected via EPMA).

Figure S1. Simplified geologic map of the eastern Sierra Nevada batholith, highlighting intrusive suites in the study area.

Figure S2. Representative images of cumulate rocks in thin section under cross polarized light (A, C, E) and back scattered electron imagery (B, D, F), showing the textures of olivine and clinopyroxene grains that were analyzed via electron probe microanaylsis.

Figure S3. Cathodoluminescence images for a subset zircon of grains from selected dated samples.

Figure S4. Weighted mean age and Wetherill concordia plots for all new U-Pb zircon geochronology samples.

Figure S5. SiO2 vs oxide plots for all mafic samples from the Eastern Sierra Nevada batholith (SNB), and granitoids from the SNB for comparison.

Figure S6. Sr/Y values vs SiO2 (wt.%) for the SNB, including samples from the NAVDAT database and samples of the mafic bodies included in this study, which include our new analyses and previous work.

Figure S7. Bulk-rock Sr/Nd vs Al/Si ratios for mafic samples.

Supplementary Figures

Figure S1

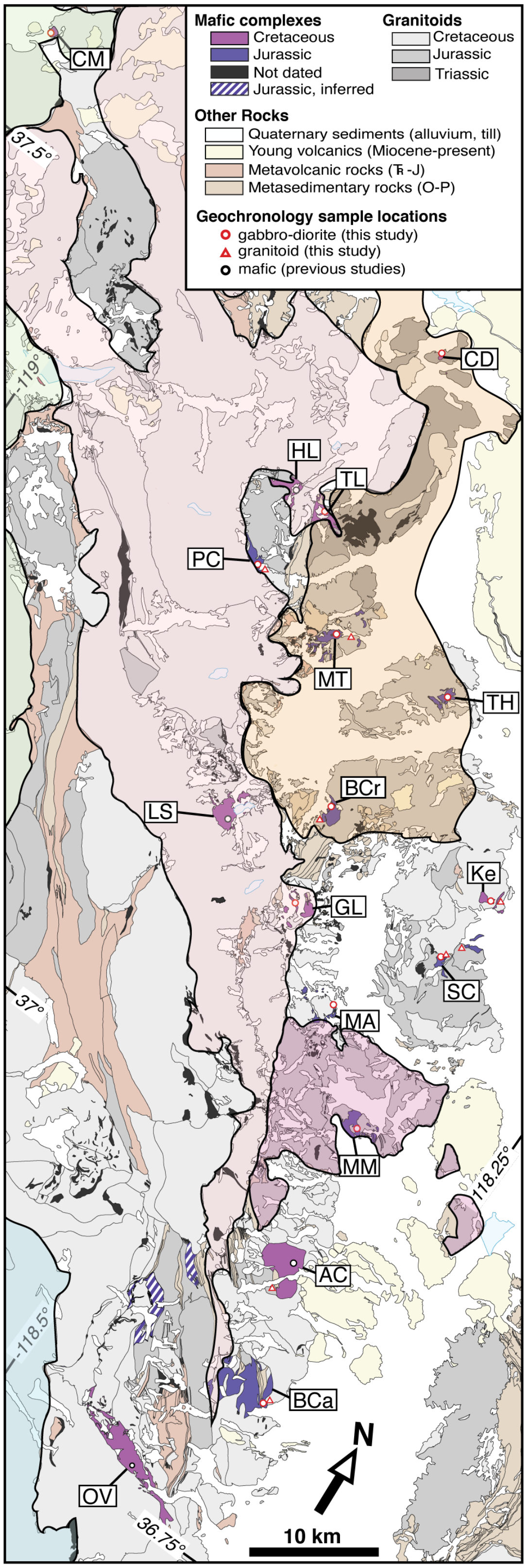

Figure S1. Simplified geologic map of the eastern Sierra Nevada batholith, highlighting intrusive suites in the study area: John Muir (Davis et al., 2012), Scheelite (Barth et al., 2011), Mount Givens (Frazer et al., 2014), Mount Whitney (Hirt, 2007), and Palisade Crest (Bateman, 1992). Names of mafic bodies are abbreviated as: CM-Cargyle Meadows, CD-Casa Diablo, HL-Hidden Lakes, TL-Tamarack Lakes, PC-Pine Creek, MT-Mount Tom, TH-Tungsten Hills, LS-Lake Sabrina, BCr-Bishop Creek, Ke-Keough, GL-Green Lake, SC-Shannon Canyon, MA-Mount Alice, MM-McMurray Meadows, AC-Armstrong Canyon, BCa-Black Canyon, and OV-Onion Valley. See Figure 1 for additional mapping references.

Figure S2

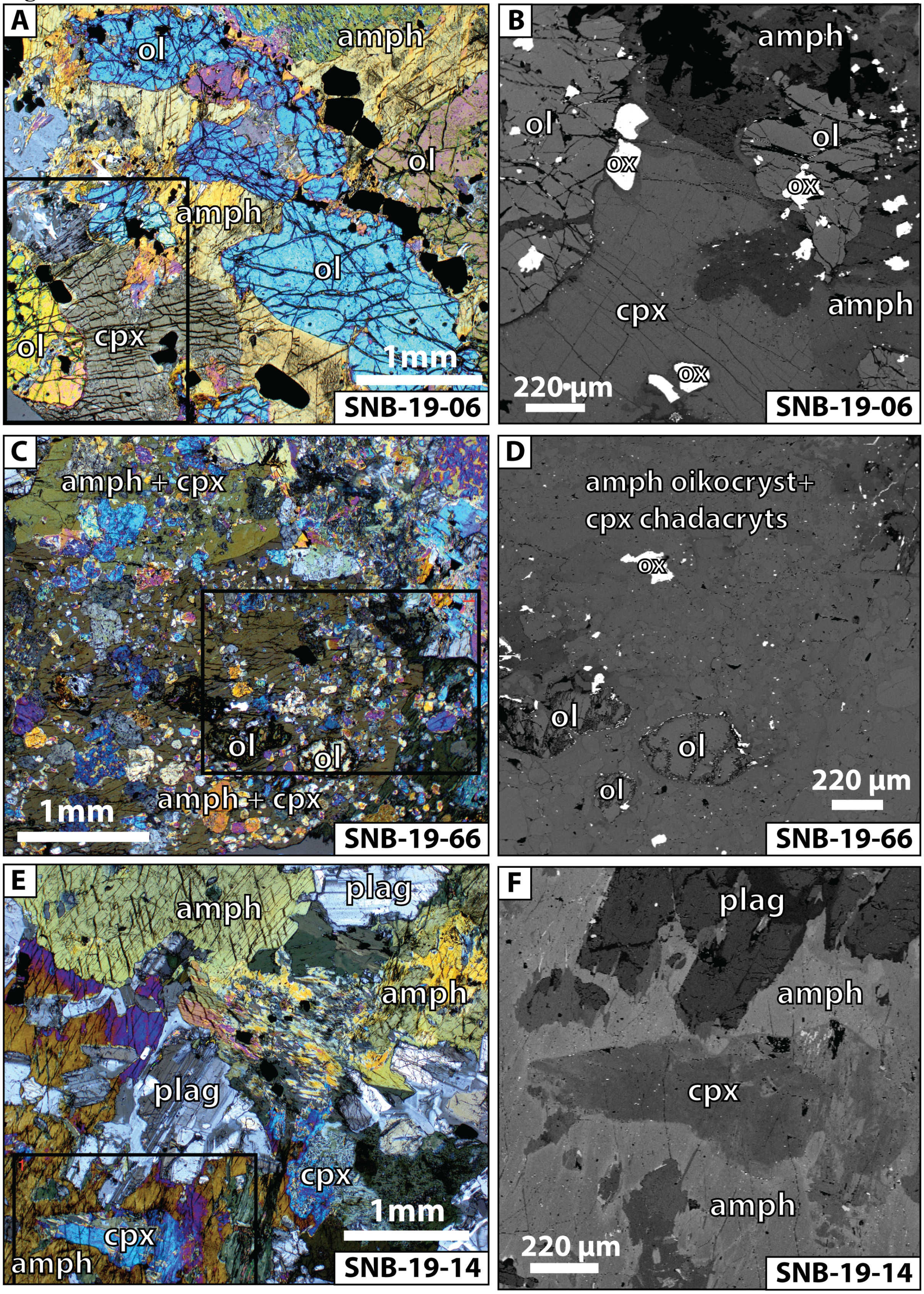
A
ol
amph
ol
amph
ol
ol
cpx
1mm
SNB-19-06
B
amph
ol
ol
ox
ox
cpx
amph
ox
220 µm
SNB-19-06
C
amph + cpx
ol
ol
amph + cpx
1mm
SNB-19-66
D
amph oikocryst+
cpx chadacryts
ox
ol
ol
ol
220 µm
SNB-19-66
E
amph
plag
amph
plag
cpx
1mm
cpx
amph
SNB-19-14
F
plag
amph
cpx
amph
220 µm
SNB-19-14

Figure S2. Representative images of cumulate rocks in thin section under cross polarized light (A, C, E) and back scattered electron imagery (B, D, F), showing the textures of olivine and clinopyroxene grains that were analyzed via electron probe microanaylsis. Mineral abbreviations are as follows: ol- olivine, amph- amphibole, cpx- clinopyroxene, ox- Fe and Fe-Ti oxides. (A) and (B) show sample SNB-19-06, an amphibole-bearing olivine websterite from the Casa Diablo mafic body. (C) and (D) show sample SNB-19-66, an amphibole-olivine gabbro from the McMurry Meadows mafic body. This sample contains abundant poikilitic amphibole grains containing olivine and fine-grained clinophyroxene chadacrysts. Similar textures (± olivine) are seen in other amphibole gabbros from McMurry Meadows, as well as Green Lake and Onion Valley gabbros. (E) and (F) shows sample SNB-19-14, an amphibole gabbro from the Cargyle Meadows mafic body. This example shows a clinopyroxene grain with an amphibole rim.

Figure S3

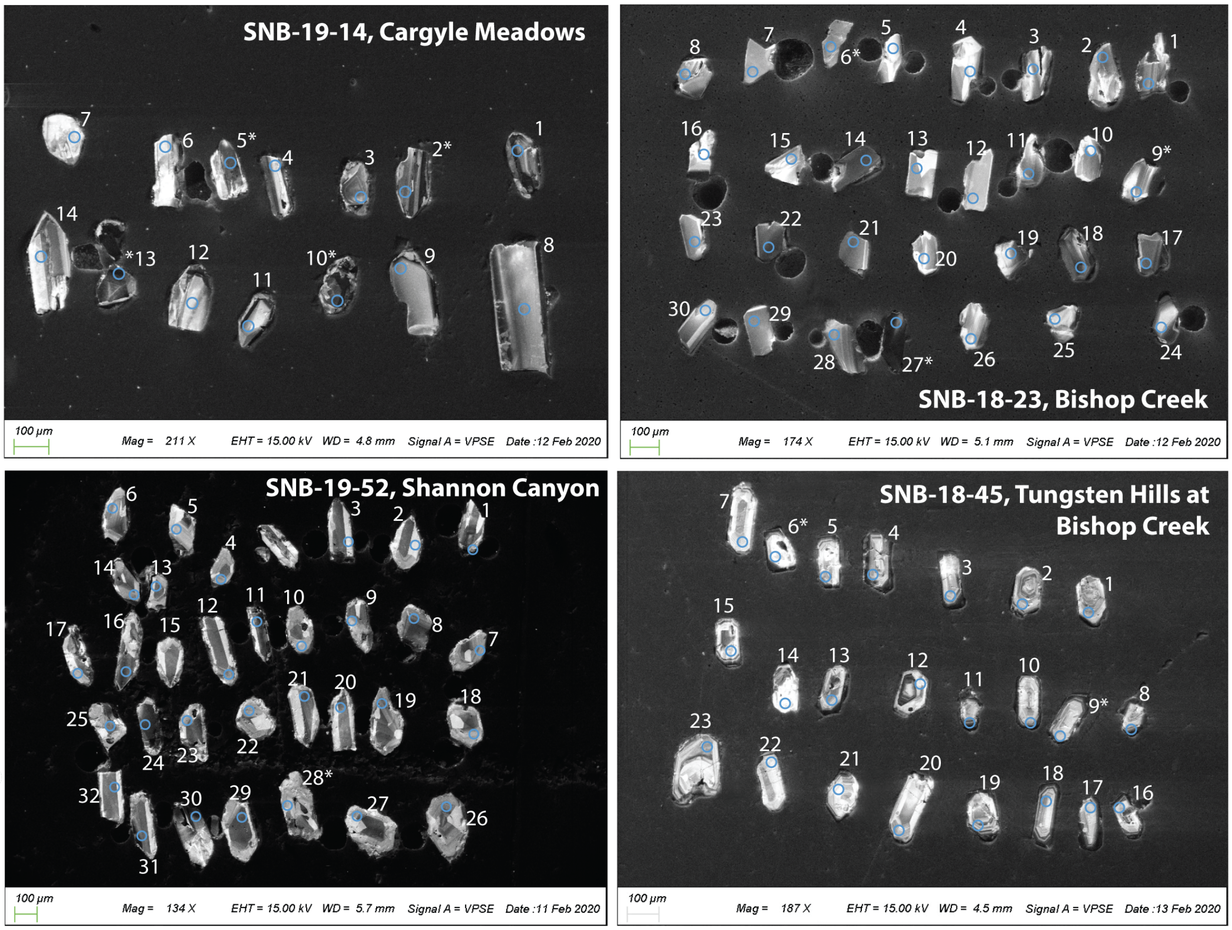

Figure S3. Cathodoluminescence images for a subset zircon of grains from selected dated samples. Grain numbers with asterisks indicate outlier or discordant grains excluded from the weighted mean age. (A) SNB-19-14 amphibole gabbro from Cargyle Meadows mafic body, some grains sector zoned and others weakly oscillatory zoned. (B) SNB-18-23 biotite gabbro from Bishop Creek mafic body with minimal zonation. Weak sector and oscillatory zoning is seen on some grains. (C) SNB-19-52 biotite rich diorite from Shannon Canyon mafic body with pronounced sector zoning. (D) SNB-18-45 quartz monzonite adjacent to Bishop Creek, mapped as the Tungsten Hills Quartz Monzonite. Similar to most of the dated granitoids in this study, most grains show concentric oscillatory zoning.

Figure S4

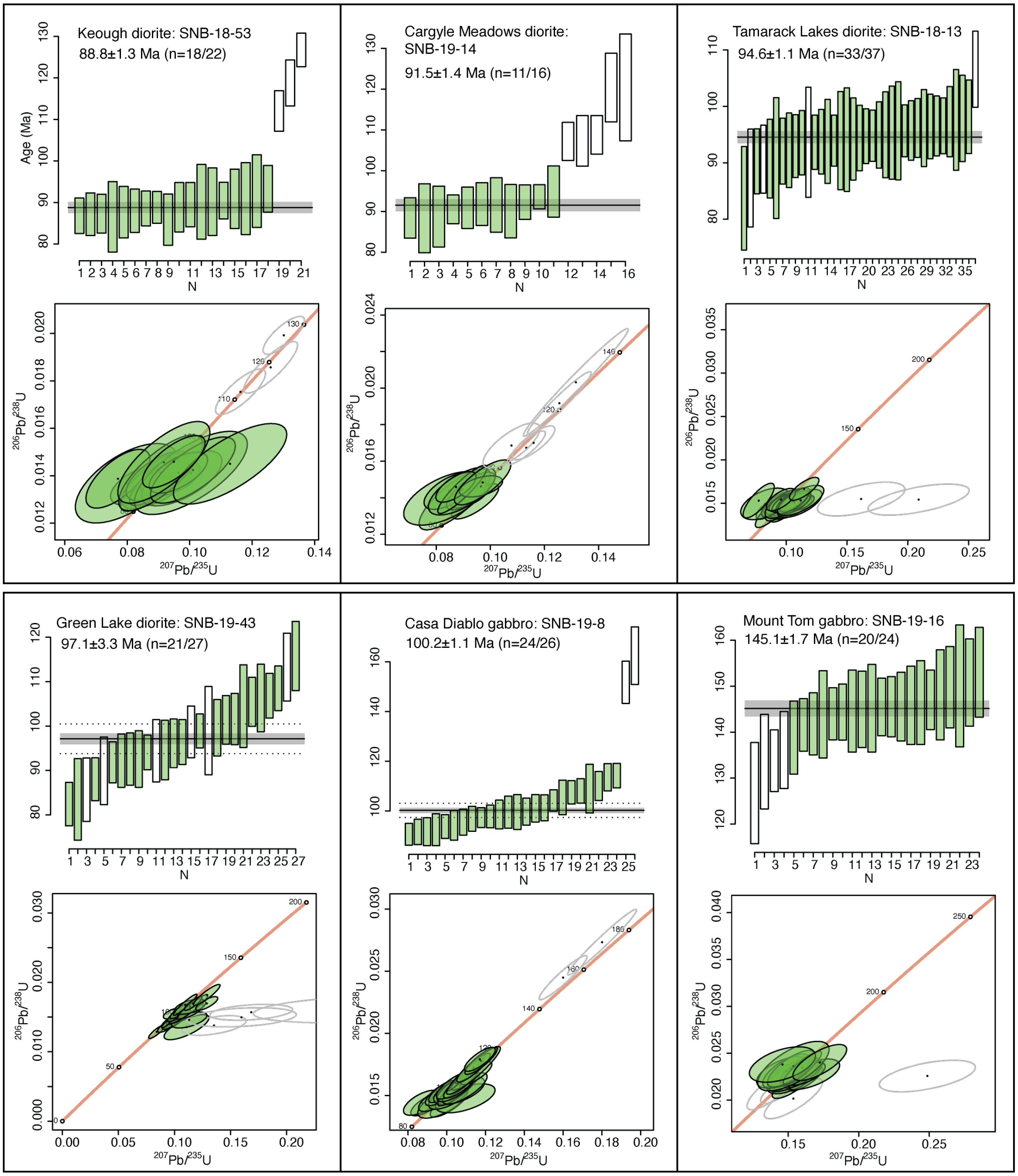

Keough diorite: SNB-18-53
88.8±1.3 Ma (n=18/22)
Cargyle Meadows diorite:
SNB-19-14
91.5±1.4 Ma (n=11/16)
Tamarack Lakes diorite: SNB-18-13
94.6±1.1 Ma (n=33/37)
Green Lake diorite: SNB-19-43
97.1±3.3 Ma (n=21/27)
Casa Diablo gabbro: SNB-19-8
100.2±1.1 Ma (n=24/26)
Mount Tom gabbro: SNB-19-16
145.1±1.7 Ma (n=20/24)
Age (Ma)
N
$^{206}Pb/^{238}U$
$^{207}Pb/^{235}U$

Figure S4 (cont.)

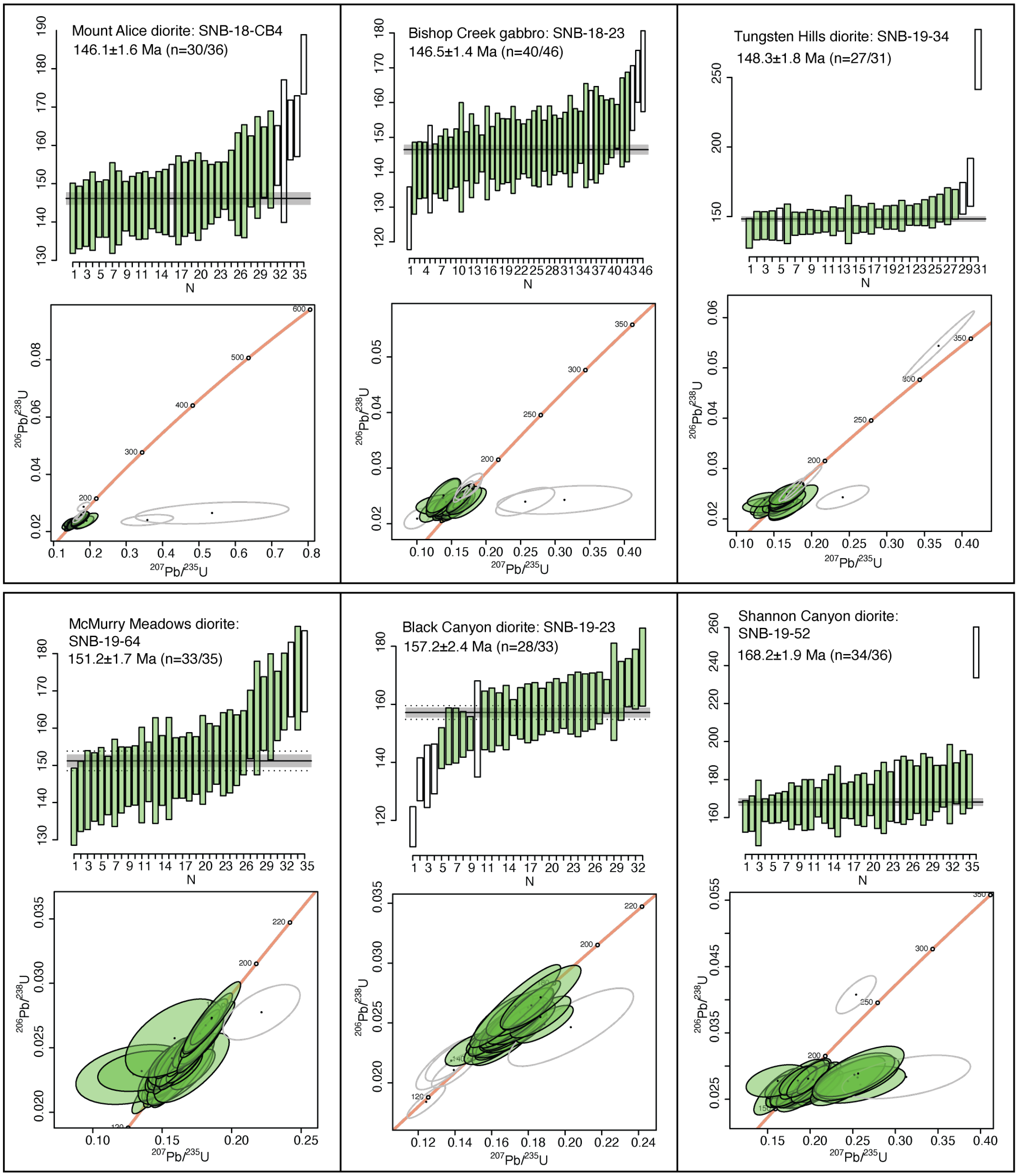

Figure S4 (cont.)

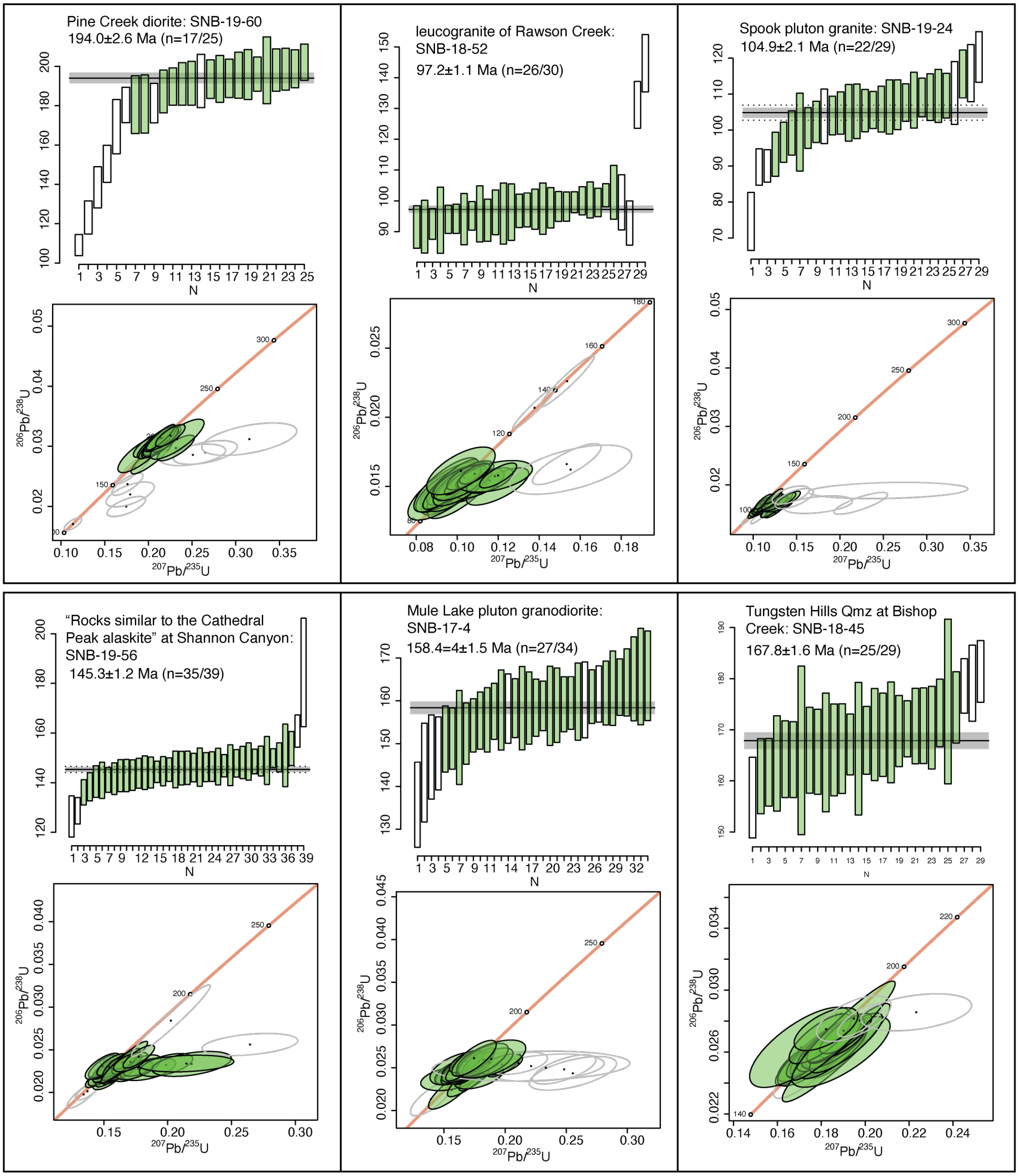

Figure S4 (cont.)

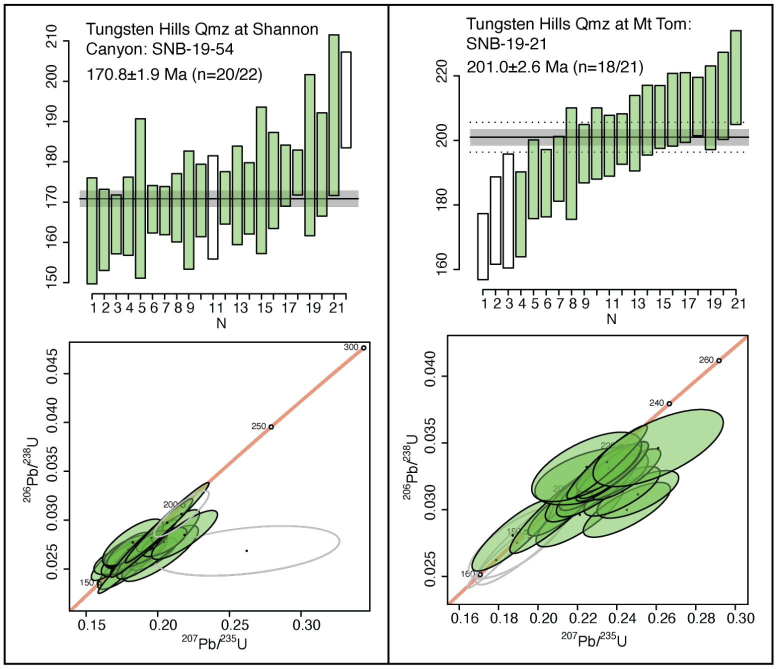

Figure S4. Weighted mean age and Wetherill concordia plots for all new U-Pb zircon geochronology samples. Green bars and ellipses are analyses that are included in the age calculation. Unfilled bars and ellipses are excluded grains that are considered inherited, discordant, or outliers based on the IsoplotR Chauvenet's criterion for outlier identification (Vermeesch 2018). Horizonal black lines in weighted mean age plots are the sample weighted mean age, gray bar is the 2σ confidence interval, and the error given with the age at the top of each panel is 2σ of the acceptable (i.e., non-excluded) zircon analyses. All plots where generated using IsoplotR (Vermeesch 2018).

Figure S5

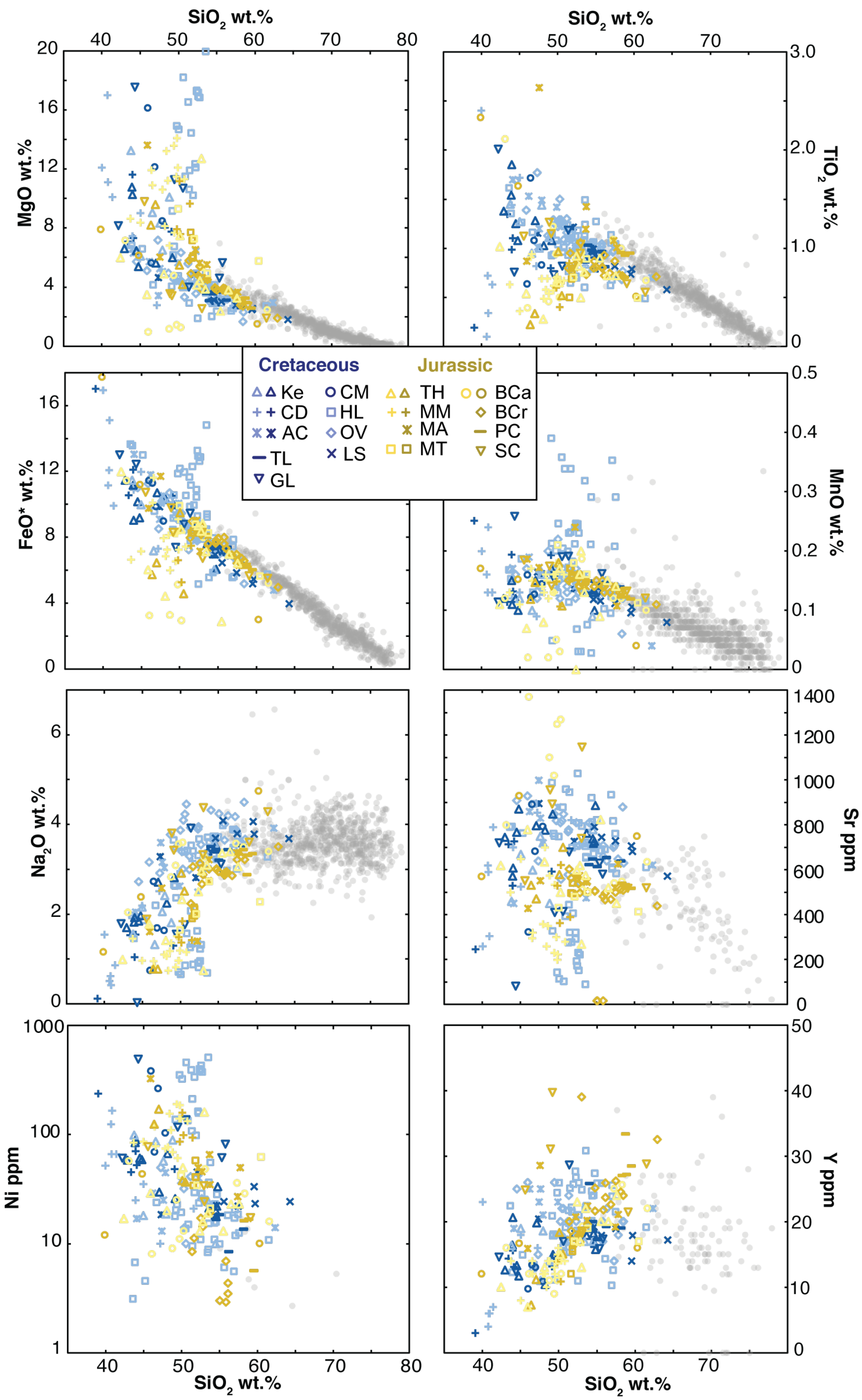

Figure S5. SiO_2 vs oxide plots for all mafic samples from the Eastern Sierra Nevada batholith (SNB), and granitoids from the SNB for comparison. Yellow symbols are Jurassic bodies, and blue symbols are Cretaceous intrusions. Darker colored symbols are new to this study, and lighter symbols have been previously published. Onion Valley samples are from Sisson et al. (1996), Hidden Lakes samples are from Lewis et al. (2021), and all other samples not from this study are from Frost (1987).

Figure S6

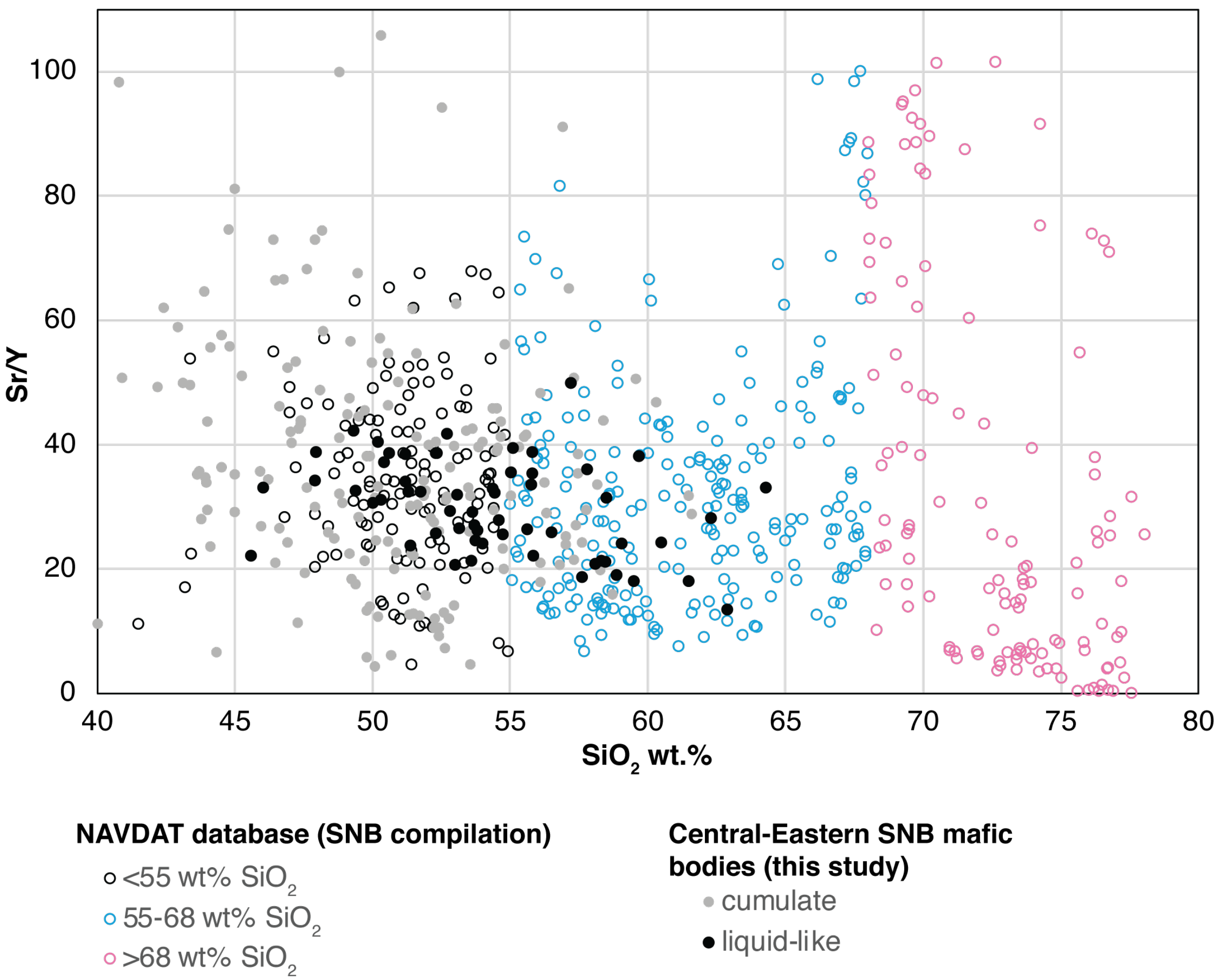

Figure S6. Sr/Y values vs SiO_2 (wt.%) for the SNB, including samples from the NAVDAT database (open circles; http://www.navdat.org) and samples of the mafic bodies included in this study, which include our new analyses and previous work (Frost 1987; Sisson et al., 1996; Lewis et al., 2021) (filled circles). The Profeta et al. (2015) crustal thickness proxy model is calibrated for rocks with 55 to 68 wt.% SiO_2 (blue circles), however we note that the range of Sr/Y values for samples with 45 to 55 wt.% SiO_2 in the SNB is roughly equivalent to that of intermediate samples (<68 wt.%), and there is negligible variation of Sr/Y with SiO_2 within the range of 45 to 68 wt.% SiO_2. In particular, the range of Sr/Y values for liquid-like samples in the mafic bodies (black cicles) is more constrained than the full range of mafic samples, and is consistent with intermediate samples from the SNB. Thus, mafic liquids, in addition to intermediate samples, may reliably record crustal thicknesses in the SNB.

Figure S7

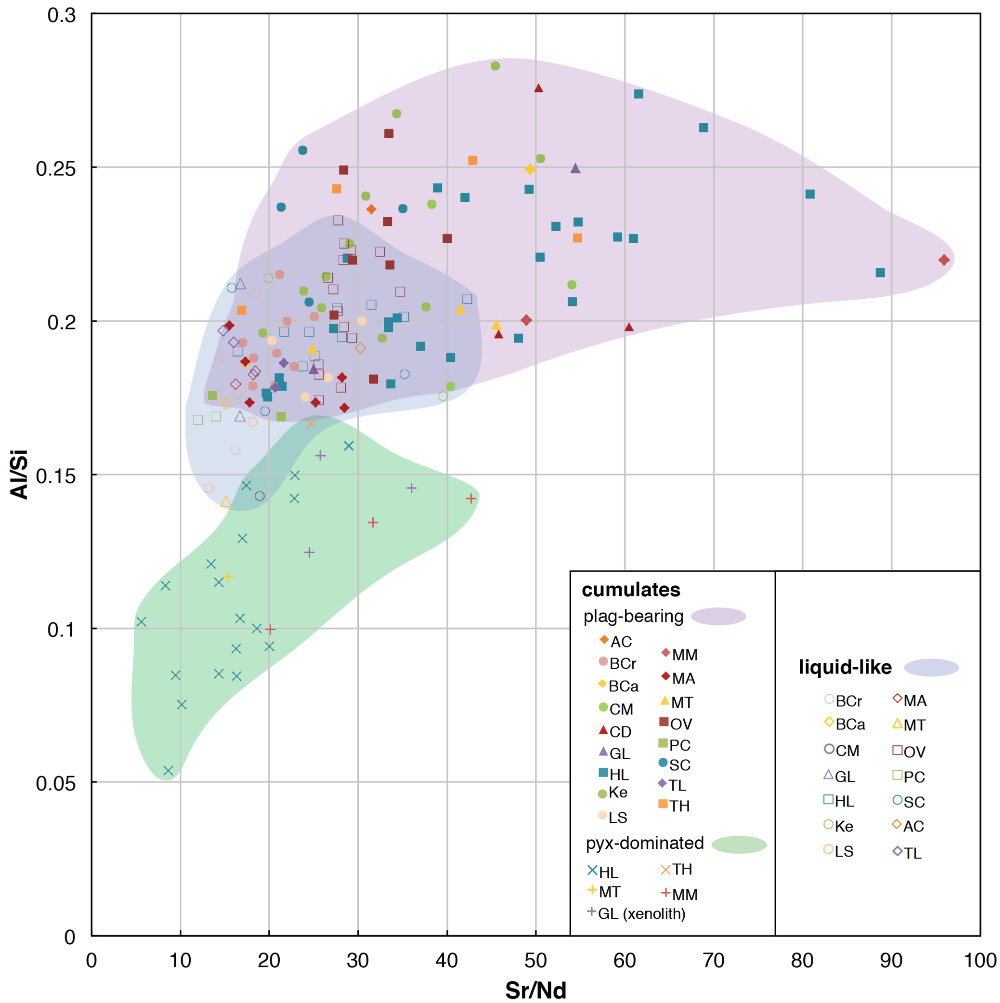

Figure S7. Bulk-rock Sr/Nd vs Al/Si ratios for mafic samples in this study and in Lewis et al. (2021). Shaded fields outline the areas where cumulate and melt-like samples are found. The elemental ratios shown indicate accumulation of plagioclase, which causes an increase in both Al/Si and Sr/Nd. As the pyroxene-dominated samples contain minimal accumulated plagioclase, these samples are classified as cumulates based on textural evidence and bulk-rock Mg#s greater than the parental melt for each body, rather than using elemental ratios. As the parental melt compositions are likely variable between each mafic body, there is considerable overlap between the melt-like and plagioclase-bearing cumulate fields. However, within each body, melt-like samples have lower Al/Si and Sr/Nd ratios than samples of cumulative origin. We also take textural evidence (dike, pillow, or fine-grained rocks) into account to classify a sample as melt-like. Both elemental ratios are proxies for accumulation of plagioclase, so rock types dominated by pyroxene accumulation (norite, clinopyroxene-rich gabbro, peridotite, and a clinopyroxenite xenolith), have low Sr/Nd and Al/Si despite their cumulate textures.

References Cited in the Supplementary Material

Bateman, P. C., 1992, Plutonism in the central part of the Sierra Nevada batholith, California, USGS Professional Paper, US Government Printing Office, v. 1483.

Barth, A. P., Walker, J. D., Wooden, J. L., Riggs, N. R., & Schweickert, R. A. (2011). Birth of the Sierra Nevada magmatic arc: Early Mesozoic plutonism and volcanism in the east-central Sierra Nevada of California. Geosphere, v. 7, no. 4, p. 877-897.

Davis, J. W., Coleman, D. S., Gracely, J. T., Gaschnig, R., & Stearns, M. (2012). Magma accumulation rates and thermal histories of plutons of the Sierra Nevada batholith, CA. Contributions to Mineralogy and Petrology, v. 163, no. 3, p. 449-465.

Frazer, R. E., Coleman, D. S., & Mills, R. D. (2014). Zircon U-Pb geochronology of the Mount Givens Granodiorite: Implications for the genesis of large volumes of eruptible magma. Journal of Geophysical Research: Solid Earth, v. 119, no. 4, p. 2907-2924.

Frost, T. P., 1987, Sample localities, radiometric ages, descriptions, and major-and trace-element abundances of Late Jurassic mafic plutonic rocks, eastern Sierra Nevada, California, Department of the Interior, US Geological Survey.

Hirt, W. H. (2007). Petrology of the Mount Whitney Intrusive Suite, eastern Sierra Nevada, California: Implications for the emplacement and differentiation of composite felsic intrusions. Geological Society of America Bulletin, v. 119, no. 9-10, p. 1185-1200.

Lewis, M. J., Bucholz, C. E., & Jagoutz, O. E. (2021). Evidence for polybaric fractional crystallization in a continental arc: Hidden Lakes mafic complex, Sierra Nevada batholith, California. Contributions to Mineralogy and Petrology, 176(11), 1-27.

Sisson, T., Grove, T., and Coleman, D., 1996, Hornblende gabbro sill complex at Onion Valley, California, and a mixing origin for the Sierra Nevada batholith: Contributions to Mineralogy and Petrology, v. 126, no. 1-2, p. 81-108.

Vermeesch, P., 2018, IsoplotR: A free and open toolbox for geochronology: Geoscience Frontiers, v. 9, no. 5, p. 1479-1493.